

# Breakdown of Fourfold Symmetry in Diagonal Incommensurate Magnetic Peaks

Hiroyuki YAMASE\*

*RIKEN (The Institute of Physical and Chemical Research), Wako, Saitama 351-0198*

(Received October 11, 2001)

In the slave-boson mean-field approximation to the two-dimensional  $t$ - $J$  model, the RPA spin excitation spectrum  $\text{Im}\chi(\mathbf{q}, \omega)$  shows the diagonal incommensurate magnetic peaks that have fourfold symmetry around  $(\pi, \pi)$ . It is found in this paper that such fourfold symmetry can be broken drastically by the inclusion of a weak  $c$ -axis dispersion. This finding is discussed on a possible relevance to the recently observed ‘one-dimensional-like’ diagonal incommensurate magnetic peak in  $\text{La}_{2-x}\text{Sr}_x\text{CuO}_4$ .

KEYWORDS:  $t$ - $J$  model, slave boson, interlayer hopping,  $c$ -axis dispersion, RPA, magnetic excitation, diagonal incommensurate peak, symmetry, LSCO, stripes

## §1. Introduction

Recently, elastic neutron scattering in  $\text{La}_{2-x}\text{Sr}_x\text{CuO}_4$  (LSCO) has shown the existence of a superlattice peak at  $(\pi \pm 2\pi\eta_2, \pi \mp 2\pi\eta_2, 0)$  (tetragonal notation), which is called as a *diagonal* incommensurate (DIC-) peak, in the low doping region ( $0.02 \lesssim x \lesssim 0.05$ ).<sup>1-3)</sup> The successive study has revealed that this DIC-peak lacks the fourfold symmetry around  $(\pi, \pi)$ , that is, another (appreciable) DIC-peak at  $(\pi \mp 2\pi\eta_1, \pi \mp 2\pi\eta_1, 0)$  has not been observed.<sup>3)</sup> This ‘one-dimensional-like (1d-like)’ DIC-peak has often been discussed in terms of the ‘*diagonal* spin-charge stripes’ scenario, similar to the ‘spin-charge stripes’ scenario<sup>4-7)</sup> except that the direction of the ‘charge stripes’ is rotated by  $45^\circ$  from the Cu-O bond direction. Such charge order, however, has not been detected. Theoretically, a possible formation of ‘charge stripes’ has been argued in different contexts,<sup>8,9)</sup> but remains to be clarified.

On the other hand, in this paper, leaving a possible formation of some charge ordering to a future study and assuming the uniform charge density in the slave-boson mean-field scheme to the  $t$ - $J$  model, we study effects of the interlayer hopping integral  $t_\perp$  on the (magnetic) DIC-peaks, which have fourfold symmetry around  $(\pi, \pi)$  in the calculations for the single  $\text{CuO}_2$  plane.<sup>10)</sup> We find

---

\* E-mail: yamase@riken.go.jp

a mechanism that such fourfold symmetry can be broken drastically even with small  $t_{\perp}$ . The FS we use here has fourfold symmetry. It is the form of the  $c$ -axis dispersion that is crucial to this mechanism. We show that this mechanism actually works for the  $c$ -axis dispersion that is expected for LSCO systems, but not for the  $c$ -axis dispersion proposed for  $\text{YBa}_2\text{Cu}_3\text{O}_{6+y}$  (YBCO).<sup>11)</sup> We discuss that the present finding can be another scenario for the ‘1d-like’ DIC-peak observed in LSCO.<sup>2,3)</sup>

Since the present finding can be related to LSCO systems, we first study the DIC-peaks on the basis of a currently proposed picture for LSCO, a quasi-one-dimensional (q-1d) picture of the Fermi surface (FS).<sup>12–15)</sup> This is illustrated in Fig. 1. Either of two kinds of the FSs, q-1dFS(x) or q-1dFS(y), is realized in each  $\text{CuO}_2$  plane and they are stacked alternately along the  $c$ -axis; the charge density is assumed to be uniform. The resulting FSs have fourfold symmetry as shown in Fig. 1(b). It has been shown in refs. 12 and 13 that with this picture, the apparently contradicting experimental data between the angle-resolved photoemission spectroscopy<sup>16)</sup> and the inelastic neutron scattering<sup>17)</sup> will be reconciled. We next perform the calculation for other types of FS to demonstrate some generality of the present finding.

## §2. Model and Formalism

We take a unit cell in which two  $\text{CuO}_2$  planes,  $A$ -plane and  $B$ -plane in Fig. 1(a), are included, and divide the Bravais lattice into  $A$ -sublattice and  $B$ -sublattice. The  $t$ - $J$  model is then defined as

$$\begin{aligned}
H = & - \sum_{i,j,\sigma}^A t_{ij} f_{i\sigma}^{A\dagger} b_i^A b_j^{A\dagger} f_{j\sigma}^A + J \sum_{\langle i,j \rangle}^A \mathbf{S}_i^A \cdot \mathbf{S}_j^A \\
& - \sum_{i,j,\sigma}^B t_{ij} f_{i\sigma}^{B\dagger} b_i^B b_j^{B\dagger} f_{j\sigma}^B + J \sum_{\langle i,j \rangle}^B \mathbf{S}_i^B \cdot \mathbf{S}_j^B \\
& - t_{\perp} \sum_{\substack{\langle i,j \rangle \\ i \in A, j \in B}} \left( f_{i\sigma}^{A\dagger} b_i^A b_j^{B\dagger} f_{j\sigma}^B + \text{h.c.} \right), \tag{2.1}
\end{aligned}$$

$$\begin{aligned}
\sum_{\sigma} f_{i\sigma}^{A\dagger} f_{i\sigma}^A + b_i^{A\dagger} b_i^A = 1, \quad \sum_{\sigma} f_{i\sigma}^{B\dagger} f_{i\sigma}^B + b_i^{B\dagger} b_i^B = 1 \\
\text{at each site of } A\text{- and } B\text{-sublattice,} \tag{2.2}
\end{aligned}$$

where  $f_{i\sigma}^{A(B)}$  is a fermion operator with spin  $\sigma$  on the  $A(B)$ -sublattice,  $b_i^{A(B)}$  is a boson operator with charge  $e$ , namely we adopt the slave-boson scheme.  $\mathbf{S}_i^{A(B)} = \frac{1}{2} \sum_{\alpha,\beta} f_{i\alpha}^{A(B)\dagger} \boldsymbol{\sigma}_{\alpha\beta} f_{i\beta}^{A(B)}$  is a spin operator and  $\boldsymbol{\sigma}$  is Pauli matrix.  $t_{ij} = t(t')$  is the inplane hopping integral between the first (second) nearest neighbor sites.  $J > 0$  is the superexchange coupling and  $t_{\perp}$  is the interlayer hopping integral;  $\langle i, j \rangle$  indicates that  $i$  and  $j$  are the nearest neighbor sites. The constraint eq. (2.2) excludes double occupations at every site. We neglect the interlayer magnetic coupling  $J_{\perp}$  whose order is estimated as  $\sim 5$  orders smaller than  $J$ .<sup>18–20)</sup>

Leaving the details elsewhere,<sup>13)</sup> we then obtain the mean-field Hamiltonian:

$$H_{\text{MF}} = \sum_{\mathbf{k}} \begin{pmatrix} f_{\mathbf{k}\uparrow}^{A\dagger} & f_{-\mathbf{k}\downarrow}^A & f_{\mathbf{k}\uparrow}^{B\dagger} & f_{-\mathbf{k}\downarrow}^B \end{pmatrix} \begin{pmatrix} \xi_{\mathbf{k}}^A & -\Delta_{\mathbf{k}} & \epsilon_{\mathbf{k}} & 0 \\ -\Delta_{\mathbf{k}} & -\xi_{\mathbf{k}}^A & 0 & -\epsilon_{\mathbf{k}} \\ \epsilon_{\mathbf{k}} & 0 & \xi_{\mathbf{k}}^B & -\Delta_{\mathbf{k}} \\ 0 & -\epsilon_{\mathbf{k}} & -\Delta_{\mathbf{k}} & -\xi_{\mathbf{k}}^B \end{pmatrix} \begin{pmatrix} f_{\mathbf{k}\uparrow}^A \\ f_{-\mathbf{k}\downarrow}^{A\dagger} \\ f_{\mathbf{k}\uparrow}^B \\ f_{-\mathbf{k}\downarrow}^{B\dagger} \end{pmatrix}, \quad (2.3)$$

where

$$\xi_{\mathbf{k}}^A = F(\cos k_x + \alpha \cos k_y) + F'(\cos(k_x + k_y) + \cos(k_x - k_y)) - \mu, \quad (2.4)$$

$$\xi_{\mathbf{k}}^B = F(\alpha \cos k_x + \cos k_y) + F'(\cos(k_x + k_y) + \cos(k_x - k_y)) - \mu, \quad (2.5)$$

$$\Delta_{\mathbf{k}} = -\frac{3}{4}J\Delta_0(\cos k_x - \cos k_y), \quad (2.6)$$

$$\epsilon_{\mathbf{k}} = -8t_{\perp}\delta \cos \frac{k_x}{2} \cos \frac{k_y}{2} \cos \frac{k_z}{2}. \quad (2.7)$$

In eq. (2.3), we neglect boson degree of freedom, assuming the condensation to the bottom of its band. This assumption will be reasonable at low temperature.  $\xi_{\mathbf{k}}^A$  and  $\xi_{\mathbf{k}}^B$  are the ‘q-1d’ band, as represented by  $\alpha \leq 1$ , each of which forms the q-1dFS(x) and the q-1dFS(y) in Fig. 1(a), respectively. The value of  $\alpha$  is determined by fitting the q-1dFS(x) near  $(0, \pi)$  to the observed FS segments.<sup>16)</sup>  $F$  and  $F'$  are renormalized hopping amplitudes of  $t$  and  $t'$ , respectively.  $\mu$  is the chemical potential and  $\Delta_0$  is the amplitude of the  $d$ -wave singlet order.  $\epsilon_{\mathbf{k}}$  is the  $c$ -axis dispersion, whose wavevector dependence comes from the body-centered tetragonal (bct) structure of LSCO systems, where  $A$ -sublattice and  $B$ -sublattice are relatively displaced by  $[\frac{1}{2}, \frac{1}{2}, \frac{1}{2}]$ .

After the diagonalization of the Hamiltonian eq. (2.3), we obtain the band energy

$$\lambda_{\mathbf{k}}^{\pm} = \sqrt{\left(\frac{\xi_{\mathbf{k}}^A + \xi_{\mathbf{k}}^B \pm \sqrt{D_{\mathbf{k}}}}{2}\right)^2 + \Delta_{\mathbf{k}}^2}, \quad (2.8)$$

where  $D_{\mathbf{k}} = (\xi_{\mathbf{k}}^A - \xi_{\mathbf{k}}^B)^2 + 4\epsilon_{\mathbf{k}}^2$ . In Fig. 1(b) we show the FSs. They consist of the inner FS and the outer FS, each of which is defined by  $\lambda_{\mathbf{k}}^+ = 0$  and  $\lambda_{\mathbf{k}}^- = 0$ , with  $\Delta_{\mathbf{k}} = 0$ , respectively.

Since the particle-hole scattering consists of two processes, the intraband process and the interband process, the irreducible dynamical magnetic susceptibility  $\chi_0(\mathbf{q}, \omega)$  is given by  $\chi_0(\mathbf{q}, \omega) = \chi_0^{\text{intra}}(\mathbf{q}, \omega) + \chi_0^{\text{inter}}(\mathbf{q}, \omega)$ :

$$\begin{aligned} \chi_0^{\text{intra}}(\mathbf{q}, \omega) &= \frac{1}{16NN_z} \sum_{\mathbf{k}} \left[ C_{\mathbf{k}, \mathbf{k}+\mathbf{q}}^{1+} \left( \tanh \frac{\beta\lambda_{\mathbf{k}}^+}{2} - \tanh \frac{\beta\lambda_{\mathbf{k}+\mathbf{q}}^+}{2} \right) \frac{1}{\lambda_{\mathbf{k}}^+ + \omega + i\Gamma - \lambda_{\mathbf{k}+\mathbf{q}}^+} \right. \\ &+ \frac{1}{2} C_{\mathbf{k}, \mathbf{k}+\mathbf{q}}^{1-} \left( \tanh \frac{\beta\lambda_{\mathbf{k}}^+}{2} + \tanh \frac{\beta\lambda_{\mathbf{k}+\mathbf{q}}^+}{2} \right) \left( \frac{1}{\lambda_{\mathbf{k}}^+ + \omega + i\Gamma + \lambda_{\mathbf{k}+\mathbf{q}}^+} + \frac{1}{\lambda_{\mathbf{k}}^+ - \omega - i\Gamma + \lambda_{\mathbf{k}+\mathbf{q}}^+} \right) \\ &+ C_{\mathbf{k}, \mathbf{k}+\mathbf{q}}^{2+} \left( \tanh \frac{\beta\lambda_{\mathbf{k}}^-}{2} - \tanh \frac{\beta\lambda_{\mathbf{k}+\mathbf{q}}^-}{2} \right) \frac{1}{\lambda_{\mathbf{k}}^- + \omega + i\Gamma - \lambda_{\mathbf{k}+\mathbf{q}}^-} \end{aligned}$$

$$+ \frac{1}{2} C_{\mathbf{k}, \mathbf{k}+\mathbf{q}}^{2-} \left( \tanh \frac{\beta \lambda_{\mathbf{k}}^-}{2} + \tanh \frac{\beta \lambda_{\mathbf{k}+\mathbf{q}}^-}{2} \right) \left( \frac{1}{\lambda_{\mathbf{k}}^- + \omega + i\Gamma + \lambda_{\mathbf{k}+\mathbf{q}}^-} + \frac{1}{\lambda_{\mathbf{k}}^- - \omega - i\Gamma + \lambda_{\mathbf{k}+\mathbf{q}}^-} \right) \quad (2.9)$$

and

$$\begin{aligned} \chi_0^{\text{inter}}(\mathbf{q}, \omega) &= \frac{1}{16NN_z} \\ &\times \sum_{\mathbf{k}} \left[ C_{\mathbf{k}, \mathbf{k}+\mathbf{q}}^{3+} \left( \tanh \frac{\beta \lambda_{\mathbf{k}}^+}{2} - \tanh \frac{\beta \lambda_{\mathbf{k}+\mathbf{q}}^+}{2} \right) \left( \frac{1}{\lambda_{\mathbf{k}}^+ + \omega + i\Gamma - \lambda_{\mathbf{k}+\mathbf{q}}^+} + \frac{1}{\lambda_{\mathbf{k}}^+ - \omega - i\Gamma - \lambda_{\mathbf{k}+\mathbf{q}}^+} \right) \right. \\ &\left. + C_{\mathbf{k}, \mathbf{k}+\mathbf{q}}^{3-} \left( \tanh \frac{\beta \lambda_{\mathbf{k}}^+}{2} + \tanh \frac{\beta \lambda_{\mathbf{k}+\mathbf{q}}^-}{2} \right) \left( \frac{1}{\lambda_{\mathbf{k}}^+ + \omega + i\Gamma + \lambda_{\mathbf{k}+\mathbf{q}}^-} + \frac{1}{\lambda_{\mathbf{k}}^+ - \omega - i\Gamma + \lambda_{\mathbf{k}+\mathbf{q}}^-} \right) \right] \quad (2.10) \end{aligned}$$

Here  $2N_z$  ( $N$ ) is the total number of  $\text{CuO}_2$  planes (lattice sites in each  $\text{CuO}_2$  plane) and the  $\mathbf{k}$ -summation is taken in the region,  $-\pi \leq k_x, k_y, k_z \leq \pi$ .  $\beta^{-1} = T$  is temperature,  $\Gamma$  is a positive infinitesimal. The coherence factors are given by

$$\begin{aligned} C_{\mathbf{k}, \mathbf{k}+\mathbf{q}}^{1\pm} &= \frac{1}{2} \left( 1 + \frac{(\xi_{\mathbf{k}}^A - \xi_{\mathbf{k}}^B)(\xi_{\mathbf{k}+\mathbf{q}}^A - \xi_{\mathbf{k}+\mathbf{q}}^B) + 4\epsilon_{\mathbf{k}}\epsilon_{\mathbf{k}+\mathbf{q}}}{\sqrt{D_{\mathbf{k}}D_{\mathbf{k}+\mathbf{q}}}} \right) \\ &\times \left( 1 \pm \frac{(\xi_{\mathbf{k}}^A + \xi_{\mathbf{k}}^B + \sqrt{D_{\mathbf{k}}})(\xi_{\mathbf{k}+\mathbf{q}}^A + \xi_{\mathbf{k}+\mathbf{q}}^B + \sqrt{D_{\mathbf{k}+\mathbf{q}}}) + 4\Delta_{\mathbf{k}}\Delta_{\mathbf{k}+\mathbf{q}}}{4\lambda_{\mathbf{k}}^+\lambda_{\mathbf{k}+\mathbf{q}}^+} \right), \quad (2.11) \end{aligned}$$

$$\begin{aligned} C_{\mathbf{k}, \mathbf{k}+\mathbf{q}}^{2\pm} &= \frac{1}{2} \left( 1 + \frac{(\xi_{\mathbf{k}}^A - \xi_{\mathbf{k}}^B)(\xi_{\mathbf{k}+\mathbf{q}}^A - \xi_{\mathbf{k}+\mathbf{q}}^B) + 4\epsilon_{\mathbf{k}}\epsilon_{\mathbf{k}+\mathbf{q}}}{\sqrt{D_{\mathbf{k}}D_{\mathbf{k}+\mathbf{q}}}} \right) \\ &\times \left( 1 \pm \frac{(\xi_{\mathbf{k}}^A + \xi_{\mathbf{k}}^B - \sqrt{D_{\mathbf{k}}})(\xi_{\mathbf{k}+\mathbf{q}}^A + \xi_{\mathbf{k}+\mathbf{q}}^B - \sqrt{D_{\mathbf{k}+\mathbf{q}}}) + 4\Delta_{\mathbf{k}}\Delta_{\mathbf{k}+\mathbf{q}}}{4\lambda_{\mathbf{k}}^-\lambda_{\mathbf{k}+\mathbf{q}}^-} \right), \quad (2.12) \end{aligned}$$

$$\begin{aligned} C_{\mathbf{k}, \mathbf{k}+\mathbf{q}}^{3\pm} &= \frac{1}{2} \left( 1 - \frac{(\xi_{\mathbf{k}}^A - \xi_{\mathbf{k}}^B)(\xi_{\mathbf{k}+\mathbf{q}}^A - \xi_{\mathbf{k}+\mathbf{q}}^B) + 4\epsilon_{\mathbf{k}}\epsilon_{\mathbf{k}+\mathbf{q}}}{\sqrt{D_{\mathbf{k}}D_{\mathbf{k}+\mathbf{q}}}} \right) \\ &\times \left( 1 \pm \frac{(\xi_{\mathbf{k}}^A + \xi_{\mathbf{k}}^B + \sqrt{D_{\mathbf{k}}})(\xi_{\mathbf{k}+\mathbf{q}}^A + \xi_{\mathbf{k}+\mathbf{q}}^B - \sqrt{D_{\mathbf{k}+\mathbf{q}}}) + 4\Delta_{\mathbf{k}}\Delta_{\mathbf{k}+\mathbf{q}}}{4\lambda_{\mathbf{k}}^+\lambda_{\mathbf{k}+\mathbf{q}}^-} \right). \quad (2.13) \end{aligned}$$

In the numerical calculation of  $\chi_0(\mathbf{q}, \omega)$ , we set  $\Gamma = 0.01J$  (this may set the energy resolution) and  $T = 0.01J$ , where the  $d$ -wave singlet pairing (the  $d$ -wave resonating-valence-bond ( $d$ -RVB)) state is stabilized. The  $\mathbf{k}$ -summation is replaced as  $\frac{1}{NN_z} \sum \rightarrow \frac{1}{N_z} \sum_{k_z} \int_{-\pi}^{\pi} \frac{dk_x dk_y}{(2\pi)^2}$ , and the value of  $N_z$  is taken to be 12 to save computing time. The momentum  $k_z$  is then discrete with an interval  $2\pi/N_z$ . From the sequence of the calculations with  $N_z = 1, 4, 8, 12, 25$ , we checked that the overall  $\mathbf{q}$ -dependence of  $\chi_0(\mathbf{q}, \omega)$  does not depend on  $N_z$  for  $N_z \geq 8$ .

The ‘RPA’ dynamical magnetic susceptibility is obtained as

$$\chi(\mathbf{q}, \omega) = \frac{\chi_0(\mathbf{q}, \omega)}{1 + 2rJ(\mathbf{q})\chi_0(\mathbf{q}, \omega)}, \quad (2.14)$$

where  $J(\mathbf{q}) = J(\cos q_x + \cos q_y)$  and we introduce a numerical factor  $r$  for convenience. In the RPA, where  $r = 1$ ,  $\chi(\mathbf{q}, 0)$  diverges at low temperature in a wide doping region. This magnetic instability will be an artifact, since such divergence of  $\chi(\mathbf{q}, 0)$  will be suppressed by higher order corrections to  $\chi_0(\mathbf{q}, \omega)$ . This aspect we take into account phenomenologically by reducing the value of  $r$  to 0.35. As a result, the divergence of  $\chi(\mathbf{q}, 0)$  is limited to the doping region  $\delta \lesssim 0.02$  in the  $d$ -RVB state.

### §3. Results

In Fig. 2, we show the  $\mathbf{q}$ -dependence of  $\text{Im}\chi(\mathbf{q}, \omega)$  for several choices of  $t_\perp$ ; the scan direction is taken to cross the DIC-peak positions,  $\mathbf{q}_1^{\text{DIC}} = (\pi \mp 2\pi\eta_1, \pi \mp 2\pi\eta_1, 0)$  and  $\mathbf{q}_2^{\text{DIC}} = (\pi \pm 2\pi\eta_2, \pi \mp 2\pi\eta_2, 0)$ . For  $t_\perp = 0$ , we see the DIC-peaks have fourfold symmetry around  $(\pi, \pi)$ . However, once  $t_\perp$  is introduced, such fourfold symmetry is broken drastically, that is, the DIC-peak at  $\mathbf{q}_1^{\text{DIC}}$  is largely suppressed while the DIC-peak at  $\mathbf{q}_2^{\text{DIC}}$  does not change at all. This symmetry breaking itself is not surprising since  $\chi_0(\mathbf{q}, \omega)$  is not symmetric under the transformation  $q_x \rightarrow 2\pi - q_x$  for the present  $c$ -axis dispersion, that is, it is not a symmetry transformation of the present system with a bct lattice structure.<sup>21)</sup> The point is that this symmetry breaking is drastic even with small  $t_\perp$ .

We first note that the band dispersions  $\lambda_{\mathbf{k}}^\pm$ , and thus the FSs, have the  $2\pi$ -periodicity. It is the coherence factors (2.11)-(2.13) that break the symmetry of  $\chi_0(\mathbf{q}, \omega)$  under  $q_x \rightarrow 2\pi - q_x$ . Since in the  $d$ -RVB state the low-energy particle-hole scattering processes are limited to the vicinity of the  $d$ -wave gap nodes on the FSs, such processes are dominant contributions to  $\chi_0(\mathbf{q}, \omega)$ . For these processes, eqs. (2.11)-(2.13) can be reduced to

$$C_{\mathbf{k}, \mathbf{k}+\mathbf{q}}^{1\pm} \sim \left(1 + \text{sign}(\epsilon_{\mathbf{k}}\epsilon_{\mathbf{k}+\mathbf{q}})\right) \times \left(1 \pm \frac{\dots}{4\lambda_{\mathbf{k}}^+\lambda_{\mathbf{k}+\mathbf{q}}^+}\right), \quad (3.1)$$

$$C_{\mathbf{k}, \mathbf{k}+\mathbf{q}}^{2\pm} \sim \left(1 + \text{sign}(\epsilon_{\mathbf{k}}\epsilon_{\mathbf{k}+\mathbf{q}})\right) \times \left(1 \pm \frac{\dots}{4\lambda_{\mathbf{k}}^-\lambda_{\mathbf{k}+\mathbf{q}}^-}\right), \quad (3.2)$$

$$C_{\mathbf{k}, \mathbf{k}+\mathbf{q}}^{3\pm} \sim \left(1 - \text{sign}(\epsilon_{\mathbf{k}}\epsilon_{\mathbf{k}+\mathbf{q}})\right) \times \left(1 \pm \frac{\dots}{4\lambda_{\mathbf{k}}^+\lambda_{\mathbf{k}+\mathbf{q}}^-}\right), \quad (3.3)$$

since the factor  $\xi_{\mathbf{k}}^{\text{A}} - \xi_{\mathbf{k}}^{\text{B}}$  has the same form as  $\Delta_{\mathbf{k}}$  as seen from eqs. (2.4)-(2.6). Here we omit the numerator in the second factor in each expression, which is the same as that in eqs. (2.11)-(2.13), respectively.  $\chi_0^{\text{intra}}(\mathbf{q}, \omega)$  is thus proportional to  $\chi_0^{\text{intra}}(\mathbf{q}, \omega) \propto \sum_{\mathbf{k}} (1 + \text{sign}(\epsilon_{\mathbf{k}}\epsilon_{\mathbf{k}+\mathbf{q}})) \times \dots$ , and similarly  $\chi_0^{\text{inter}}(\mathbf{q}, \omega) \propto \sum_{\mathbf{k}} (1 - \text{sign}(\epsilon_{\mathbf{k}}\epsilon_{\mathbf{k}+\mathbf{q}})) \times \dots$ . Note that the former (latter) consists of the

scattering processes with  $\epsilon_{\mathbf{k}}\epsilon_{\mathbf{k}+\mathbf{q}} > 0 (< 0)$ . In Fig. 1(b), the possible main low-energy scattering processes for the DIC-peak at  $\mathbf{q} = \mathbf{q}_1^{\text{DIC}}$  are shown for  $k_z = 0$ . For these processes, the sign of  $\epsilon_{\mathbf{k}}\epsilon_{\mathbf{k}+\mathbf{q}}$  is positive. By transforming  $q_x \rightarrow 2\pi - q_x$  and  $k_x \rightarrow -k_x$ , the possible main scattering processes for the DIC-peak at  $\mathbf{q} = \mathbf{q}_2^{\text{DIC}}$  are obtained; the sign of  $\epsilon_{\mathbf{k}}\epsilon_{\mathbf{k}+\mathbf{q}}$  is then negative. These hold for other values of  $k_z$ .<sup>22)</sup> Thus, the DIC-peak at  $\mathbf{q}_1^{\text{DIC}}$  comes mainly from the intraband process, whereas the DIC-peak at  $\mathbf{q}_2^{\text{DIC}}$  comes mainly from the interband process. For the intraband process, there exist two different (inplane) scattering wavevectors when  $k_z$  is fixed as shown in Fig. 1(b), and these wavevectors change with different  $k_z$ . Since  $k_z$  is an integral variable, the resulting DIC-peak at  $\mathbf{q}_1^{\text{DIC}}$  is largely suppressed and broadened as shown in Fig. 2. On the other hand, for the interband process, the (inplane) scattering wavevectors are almost the same for different values of  $k_z$ . This leads to the sharp DIC-peak at  $\mathbf{q}_2^{\text{DIC}}$  independent of  $t_{\perp}$  (Fig. 2). This qualitative difference between the intraband process and the interband process causes the drastic breaking of fourfold symmetry in the DIC-peaks.

The condition for the present mechanism to work is, therefore, given by the following factors. These factors should be satisfied for the main low-energy scattering processes contributed to the DIC-peaks.

(F1) The coherence factors of  $\chi_0(\mathbf{q}, \omega)$  can be reduced to eqs. (3.1)-(3.3).

(F2) The  $c$ -axis dispersion  $\epsilon_{\mathbf{k}+\mathbf{q}}$  has an opposite sign between  $\mathbf{q} = \mathbf{q}_1^{\text{DIC}}$  and  $\mathbf{q}_2^{\text{DIC}}$ .

(F3) The sign of  $\epsilon_{\mathbf{k}}\epsilon_{\mathbf{k}+\mathbf{q}}$  is (almost) definite.

(F4) The  $c$ -axis dispersion does not vanish, otherwise there is no difference between the intraband process and the interband process.

To see the implication of the above mechanism, we next investigate (i)  $\delta$ -dependence and  $\omega$ -dependence, (ii)  $q_z$ -dependence and other quadrants in the inplane momentum space, (iii) other  $c$ -axis dispersions and (iv) effects of the  $d$ -wave gap. Hereafter, we fix the value of  $t_{\perp}$  to  $0.05t (= 0.2J)$  so that the band width of  $\epsilon_{\mathbf{k}}$  is about 0.1 times that of  $\xi_{\mathbf{k}}^{\text{A}}$  or  $\xi_{\mathbf{k}}^{\text{B}}$ .<sup>23)</sup>

(i)  *$\delta$ -dependence and  $\omega$ -dependence.* Figure 3 shows the  $\mathbf{q}$ -dependence of  $\text{Im}\chi(\mathbf{q}, \omega)$  at several choices of  $\delta$  for  $\omega = 0.01J$ . The breaking of fourfold symmetry in the DIC-peaks becomes more prominent with larger  $\delta$ , since  $\epsilon_{\mathbf{k}}$  is proportional to  $\delta$  (eq. (2.7)) and the interlayer coupling becomes effectively larger. As  $\omega$  is increased for the fixed  $\delta$ , on the other hand, the symmetry breaking becomes weaker (Fig. 4). This is understood by noting that the present mechanism comes from the effect of the  $c$ -axis dispersion and hence works effectively below the energy scale of the  $c$ -axis dispersion.

(ii)  *$q_z$ -dependence and other quadrants in the inplane momentum space.* Figure 5(a) shows the  $q_z$ -dependence of the peak heights of the DIC-peaks at  $\mathbf{q}_1^{\text{DIC}}$  and  $\mathbf{q}_2^{\text{DIC}}$ . Their peak heights change with  $4\pi$ -periodicity and the phase is relatively shifted by  $2\pi$ . This is because the sign of  $\epsilon_{\mathbf{k}}\epsilon_{\mathbf{k}+\mathbf{q}}$  changes under the transformation  $q_z \rightarrow q_z + 2\pi$ , that is, at  $q_z = 2\pi$ , the DIC-peak at  $\mathbf{q}_1^{\text{DIC}}$  ( $\mathbf{q}_2^{\text{DIC}}$ )

comes from the interband (intraband) process whereas at  $q_z = 0$ , the DIC-peak at  $\mathbf{q}_1^{\text{DIC}}$  ( $\mathbf{q}_2^{\text{DIC}}$ ) comes from the intraband (interband) process. In the intermediate value of  $q_z$  ( $0 < q_z < 2\pi$ ), the interband process (similarly the intraband process) contributes to both the DIC-peak at  $\mathbf{q}_1^{\text{DIC}}$  and  $\mathbf{q}_2^{\text{DIC}}$  with different weight, and the weight becomes equal at  $q_z = \pi$  where the fourfold symmetry is recovered. Figure 6 shows schematically how the symmetry of the DIC-peaks is broken in the inplane momentum space. This configuration is understood as due to the sign change of  $\epsilon_{\mathbf{k}}\epsilon_{\mathbf{k}+\mathbf{q}}$  under  $q_x \rightarrow q_x + 2\pi$  or  $q_y \rightarrow q_y + 2\pi$ .

(iii) *Other c-axis dispersions.* We consider (a)  $\epsilon_{\mathbf{k}} \propto (\cos k_x - \cos k_y)^2$ , which has been proposed for YBCO,<sup>11)</sup> and (b)  $\epsilon_{\mathbf{k}} \propto (\cos k_x - \cos k_y)^2 \cos \frac{k_x}{2} \cos \frac{k_y}{2} \cos \frac{k_z}{2}$ . The former dispersion does not satisfy the factor (F2). Hence the symmetry breaking does not take place. For the latter dispersion, the factor (F1) as well as (F4) are not satisfied since  $\epsilon_{\mathbf{k}} \approx 0$  for the main scattering processes of the DIC-peaks. Thus the DIC-peaks retain the almost fourfold symmetry.

(iv) *Effects of the d-wave gap.* We perform the calculation in the so-called uniform RVB (u-RVB) state, the state without the  $d$ -wave gap, at the same temperature  $T = 0.01J$  as in the  $d$ -RVB state. Using the  $c$ -axis dispersion eq. (2.7), we show in Fig. 7 the  $\mathbf{q}$ -dependence of  $\text{Im}\chi(\mathbf{q}, \omega)$  for several choices of  $\delta$ . The appreciable symmetry breaking is seen only at high  $\delta$ , but is much weaker than that in the  $d$ -RVB state (Fig. 3). This is understood as follows. In the u-RVB state, there occurs an additional scattering between the FSs around  $(-\pi, 0)$  and  $(0, \pi)$ , which is prevented by the  $d$ -wave gap in the  $d$ -RVB state. For this scattering process, the factor (F1) as well as (F4) are not satisfied, since at  $(-\pi, 0)$  and  $(0, \pi)$ , the magnitude of the factor  $\xi_{\mathbf{k}}^{\text{A}} - \xi_{\mathbf{k}}^{\text{B}}$  takes a maximum and the value of  $\epsilon_{\mathbf{k}}$  is zero. Thus the resulting symmetry breaking is weakened compared with that in the  $d$ -RVB state.

So far we have investigated the breaking of fourfold symmetry in the DIC-peaks on the basis of the q-1d picture of the FS (Fig. 1(a)). We next investigate other FSs: (a) the 2dFS(I) (Fig. 8(a)), which is realized in YBCO,<sup>24)</sup> and (b) the 2dFS(II) (Fig. 8(b)), which was used in the previous theoretical study for LSCO.<sup>25-27)</sup> Since the inplane band dispersion is the same between the adjacent planes, namely  $\xi_{\mathbf{k}}^{\text{A}} = \xi_{\mathbf{k}}^{\text{B}}$ , the factor (F1) is satisfied exactly. When we take the  $c$ -axis dispersion given by eq. (2.7), the factors (F2)-(F4) are satisfied also in the  $d$ -RVB state. Thus the symmetry breaking takes place as shown in Fig. 9(a). This insensitiveness to the shape of the FS is understood by noting that the DIC-peaks come mainly from the scatterings between the vicinities of the  $d$ -wave gap nodes, the local regions on the FS. In the u-RVB state, the DIC-peaks are realized in the relatively high  $\delta$  ( $\gtrsim 0.10$ ) for the 2dFS(II). Since as argued in the above (iv), the additional scattering takes place and the satisfaction of the factor (F4) is degraded, the resulting symmetry breaking (Fig. 9(b)) becomes weaker than in the  $d$ -RVB state (the comparison is made at the same  $\delta$ ), but stronger than the result (for  $\delta = 0.15$ ) shown in Fig. 7 where the satisfaction of the (F1) is degraded also. For the 2dFS(I), a broad commensurate peak is dominant and the

appreciable symmetry breaking in the DIC-peaks is not seen in Fig. 9(b).

#### §4. Conclusion and Discussion

In the slave-boson mean-field scheme to the  $t$ - $J$  model, we have studied effects of  $t_{\perp}$  on the DIC-peaks, which have fourfold symmetry around  $(\pi, \pi)$  in the absence of  $t_{\perp}$ . We have found a mechanism that such fourfold symmetry is broken drastically with a weak  $c$ -axis dispersion. The condition for this mechanism to work is given by four factors (F1)-(F4), which should be satisfied for the main low-energy scattering processes contributed to the DIC-peaks. We have demonstrated this mechanism through investigating the  $\delta$ -,  $\omega$ - and  $q_z$ -dependences of magnetic excitation spectra, the different  $c$ -axis dispersions, the effects of the  $d$ -wave gap and the different FSs.

In YBCO systems, the  $c$ -axis dispersion is believed to have the form  $\epsilon_{\mathbf{k}} \propto (\cos k_x - \cos k_y)^2$ .<sup>11)</sup> For this  $\epsilon_{\mathbf{k}}$ ,  $\chi(\mathbf{q}, \omega)$  is equivalent between  $\mathbf{q} = \mathbf{q}_1^{\text{DIC}}$  and  $\mathbf{q}_2^{\text{DIC}}$  and the factor (F2) is not satisfied. The present mechanism does not work for YBCO. On the other hand, in LSCO systems, the breaking of fourfold symmetry in the DIC-peaks or the ‘1d-like’ DIC-peak has been observed in  $0.02 \lesssim x \lesssim 0.05$ .<sup>2,3)</sup> Can we relate the present mechanism to such data?

(i) *The  $\cos \frac{k_x}{2} \cos \frac{k_y}{2} \cos \frac{k_z}{2}$ -type  $c$ -axis dispersion.* From the crystallographical viewpoint, we expect that such a  $c$ -axis dispersion is a dominant contribution in LSCO systems. Experimentally, however, the form of the  $c$ -axis dispersion has not been clarified yet.

(ii) *Existence of the spin gap.* As shown in Figs. 2, 3 and 7, the fourfold symmetry breaking is prominent only in the  $d$ -RVB state at low  $\delta$ . It is reasonable from the RVB picture<sup>28)</sup> that we expect the spin gap (or the  $d$ -wave gap) in the actual system with  $0.02 \lesssim x \lesssim 0.05$ . The existence of the spin gap in such low doping region, however, has not been clarified yet experimentally.

(iii) *Origin of the DIC-peaks.* In the present theoretical framework,<sup>13)</sup> the DIC-peaks are realized not only in the low doping region ( $\delta \lesssim 0.05$ ) but also in the high doping region ( $\delta \gtrsim 0.05$ ). Experimentally, however, the DIC-peaks have been detected only in the low doping region.<sup>1-3)</sup> This inconsistency should be resolved in a future.

Keeping in mind that the above aspects will be crucial to further discussions, we point out at present that Figs. 2, 5 and 6 do not contradict with experimental data.<sup>2,3)</sup> Thus the present mechanism can be a scenario for the observed ‘1d-like’ DIC-peak.

Here we note effects of the low-temperature orthorhombic (LTO) structure in LSCO, since the possible coupling to such lattice distortion causes the breaking of fourfold symmetry in the DIC-peaks. To investigate this, we introduce the additional parameter  $\gamma$  in eqs. (2.4) and (2.5):<sup>12)</sup>  $\cos(k_x + k_y) + \cos(k_x - k_y) \rightarrow \cos(k_x + k_y) + \gamma \cos(k_x - k_y)$  where  $\gamma < 1$ . Setting  $\gamma = 0.8$ , we calculate  $\text{Im}\chi(\mathbf{q}, \omega)$  for the *single*  $\text{CuO}_2$  plane at low  $\omega$  ( $= 0.01J$ ) for  $\delta = 0.05$ . We find that in both the  $d$ -RVB state and the  $u$ -RVB state, the DIC-peaks retain the almost fourfold symmetry. We thus expect that the LTO structure is not an essential factor to the symmetry breaking in the DIC-peaks.

We finally note the difference between the present mechanism and the ‘*diagonal* spin-charge stripes’ picture. The latter is a charge-origin scenario: the formation of a ‘*diagonal* charge stripes’ order (or its fluctuations), which will couple to the LTO lattice distortion, causes the breaking of fourfold symmetry in the (magnetic) DIC-peaks. In contrast, the present mechanism provides a spin-origin scenario. The breaking of fourfold symmetry results from the spin-spin correlation in the presence of some *c*-axis dispersion, and the LTO structure is not an essential factor. This mechanism can be another scenario for the ‘1d-like’ DIC-peak observed in LSCO.<sup>2,3)</sup>

### **Acknowledgments**

The author thanks Hiroshi Kohno for critical reading the manuscript and fruitful discussions. He is also indebted to H. Kimura, H. Kino and M. Mastuda for helpful discussions. This work is supported by a Special Postdoctoral Researchers Program from RIKEN.

- 
- 1) S. Wakimoto, G. Shirane, Y. Endoh, K. Hirota, S. Ueki, K. Yamada, R. J. Birgeneau, M. A. Kastner, Y. S. Lee, P. M. Gehring and S. H. Lee: Phys. Rev. B **60** (1999) R769.
  - 2) M. Matsuda, M. Fujita, K. Yamada, R. J. Birgeneau, M. A. Kastner, H. Hiraka, Y. Endoh, S. Wakimoto and G. Shirane: Phys. Rev. B **62** (2000) 9148.
  - 3) S. Wakimoto, R. J. Birgeneau, M. A. Kastner, Y. S. Lee, R. Erwin, P. M. Gehring, S. H. Lee, M. Fujita, K. Yamada, Y. Endoh, K. Hirota and G. Shirane: Phys. Rev. B **61** (2000) 3699.
  - 4) The ‘spin-charge stripes’ scenario has been proposed by Tranquada *et al.*<sup>5-7)</sup> to understand the elastic neutron scattering data in the Nd-doped LSCO around  $x \approx 0.12$ . In this system, some charge density modulation with the wavevectors  $(\pm 4\pi\eta, 0)$  and  $(0, \pm 4\pi\eta)$  is observed and accompanied by the incommensurate antiferromagnetic order with the wavevectors  $(\pi \pm 2\pi\eta, \pi)$  and  $(\pi, \pi \pm 2\pi\eta)$  at lower temperature.
  - 5) J. M. Tranquada, B. J. Sternlieb, J. D. Axe, Y. Nakamura and S. Uchida: Nature **375** (1995) 561.
  - 6) J. M. Tranquada, J. D. Axe, N. Ichikawa, Y. Nakamura, S. Uchida and B. Nachumi: Phys. Rev. B **54** (1996) 7489.
  - 7) J. M. Tranquada, J. D. Axe, N. Ichikawa, A. R. Moodenbaugh, Y. Nakamura and S. Uchida: Phys. Rev. Lett. **78** (1997) 338.
  - 8) V. J. Emery and S. A. Kivelson: Physica C **209** (1993) 597.
  - 9) S. R. White and D. J. Scalapino: Phys. Rev. B **61** (2000) 6320.
  - 10) H. Yamase and H. Kohno: to appear in J. Phys. Chem. Solids.
  - 11) O. K. Andersen, A. I. Liechtenstein, O. Jepsen and F. Paulsen: J. Phys. Chem. Solids **56** (1995) 1573.
  - 12) H. Yamase and H. Kohno: J. Phys. Soc. Jpn. **69** (2000) 332; H. Yamase, H. Kohno and H. Fukuyama: Physica B **284-288** (2000) 1375.
  - 13) H. Yamase and H. Kohno: J. Phys. Soc. Jpn. **70** (2001) 2733.
  - 14) H. Yamase and H. Kohno: J. Phys. Soc. Jpn. **69** (2000) 2151; H. Yamase, H. Kohno and H. Fukuyama: Physica C **341-348** (2000) 321.
  - 15) C. J. Halboth and W. Metzner: Phys. Rev. Lett. **85** (2000) 5162.
  - 16) A. Ino, C. Kim, T. Mizokawa, Z.-X. Shen, A. Fujimori, M. Takaba, K. Tamasaku, H. Eisaki and S. Uchida: J. Phys. Soc. Jpn. **68** (1999) 1496.
  - 17) K. Yamada, C. H. Lee, K. Kurahashi, J. Wada, S. Wakimoto, S. Ueki, H. Kimura, Y. Endoh, S. Hosoya, G. Shirane, R. J. Birgeneau, M. Greven, M. A. Kastner and Y. J. Kim: Phys. Rev. B **57** (1998) 6165 and references therein.
  - 18) C. J. Peters, R. J. Birgeneau, M. A. Kastner, H. Yoshizawa, Y. Endoh, J. Tranquada, G. Shirane, Y. Hidaka, M. Oda, M. Suzuki and T. Murakami: Phys. Rev. B **37** (1988) 9761.
  - 19) T. Thio, T. R. Thurston, N. W. Preyer, P. J. Picone, M. A. Kastner, H. P. Jenssen, D. R. Gabbe, C. Y. Chen, R. J. Birgeneau and A. Aharony: Phys. Rev. B **38** (1988) 905.
  - 20) K. B. Lyons, P. A. Fleury, J. P. Remeika, A. C. Cooper and T. J. Negran: Phys. Rev. B **37** (1988) 2353.
  - 21) The fourfold symmetry in the incommensurate peaks at  $(\pi \pm 2\pi\eta, \pi, q_z)$  and  $(\pi, \pi \pm 2\pi\eta, q_z)$  is not broken, since they are related each other via the symmetry transformation  $(q_x, q_y) \rightarrow (q_y, q_x)$ .
  - 22) Precisely, the present argument is broken at  $k_z \approx \pi$  where  $\epsilon_{\mathbf{k}}\epsilon_{\mathbf{k}+\mathbf{q}} \approx 0$ . The scattering processes with  $k_z \approx \pi$ , therefore, do not contribute to the breaking of the fourfold symmetry in the DIC-peaks.
  - 23) W. E. Pickett: Rev. Mod. Phys. **61** (1989) 433.
  - 24) M. C. Schabel, C.-H. Park, A. Matsuura, Z.-X. Shen, D. A. Bonn, Ruixing Liang and W. N. Hardy: Phys. Rev. B **57** (1998) 6107.

- 25) T. Tanamoto, H. Kohno and H. Fukuyama: J. Phys. Soc. Jpn. **62** (1993) 717, *ibid.* **63** (1994) 2739.
- 26) Q. Si, Y. Zha, K. Levin and J. P. Lu: Phys. Rev. B **47** (1993) 9055.
- 27) Y. Zha, K. Levin and Q. Si: Phys. Rev. B **47** (1993) 9124.
- 28) P. W. Anderson: Science **235** (1987) 1196.

*Note added in proof* —After the paper was accepted, we found that eq. (2.14) does not hold for general  $\mathbf{q}$ . The error was due to the disregard of the inequivalence between the  $A$ -sublattice and the  $B$ -sublattice, namely  $\xi_{\mathbf{k}}^A \neq \xi_{\mathbf{k}}^B$ . The correct expression is complicated and will be reported elsewhere. We here note that for the present  $\mathbf{q}$ -scan direction shown in Fig. 2, the correct expression reduces to eq. (2.14). No modifications are necessary in the calculations presented in this paper.

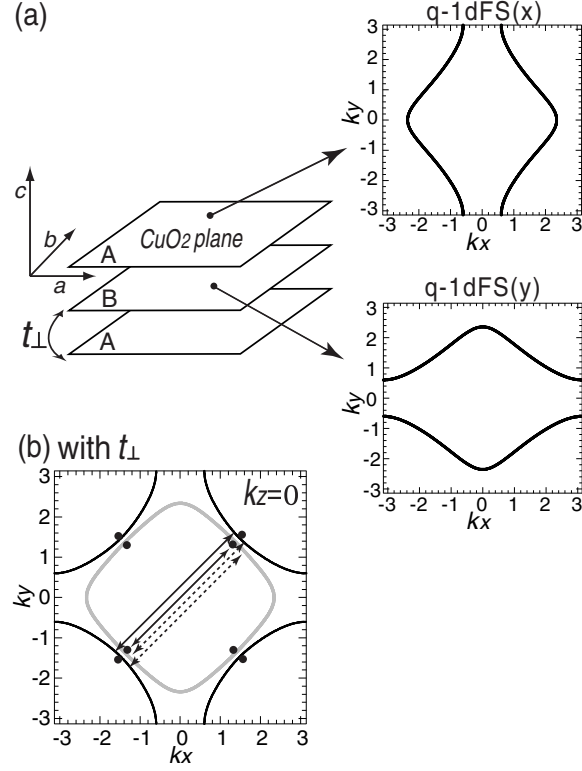


Fig. 1. (a) A quasi-one-dimensional (q-1d) picture of the FS, which has been proposed for LSCO systems:<sup>12-14)</sup> either of two kinds of FSs, q-1dFS(x) or q-1dFS(y), is realized in each CuO<sub>2</sub> plane and they are stacked alternately along the  $c$ -axis. (b) The resulting FSs in the presence of the interlayer hopping integral  $t_{\perp}$ . They consist of the inner FS (gray line) and the outer FS (solid line). The scattering processes between the  $d$ -wave gap nodes (solid circles) on the FSs, which may cause the DIC-peak at  $\mathbf{q} = (\pi \mp 2\pi\eta_1, \pi \mp 2\pi\eta_1, 0)$ , a central subject in this paper, are shown by the solid lines with arrows for the intraband scattering process and the dashed lines with arrows for the interband scattering process; these processes are drawn a little shifted away for clarity.

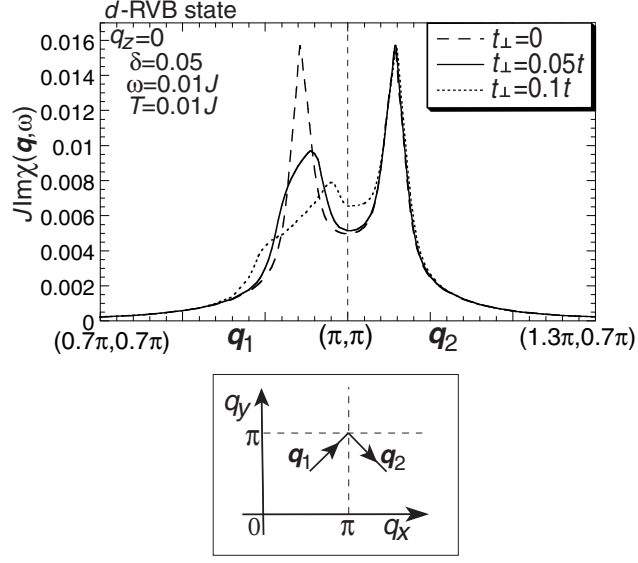


Fig. 2.  $q$ -dependence of  $\text{Im}\chi(\mathbf{q}, \omega)$  in the  $d$ -RVB state at several choices of  $t_{\perp}$  (the value of  $t$  is set to  $4J$ ). The  $q$ -scan direction is shown in the lower panel. The fourfold symmetry in the DIC-peaks at  $\mathbf{q}_1^{\text{DIC}} = (\pi \mp 2\pi\eta_1, \pi \mp 2\pi\eta_1, 0)$  and  $\mathbf{q}_2^{\text{DIC}} = (\pi \pm 2\pi\eta_2, \pi \mp 2\pi\eta_2, 0)$  is broken drastically with small  $t_{\perp}$ .

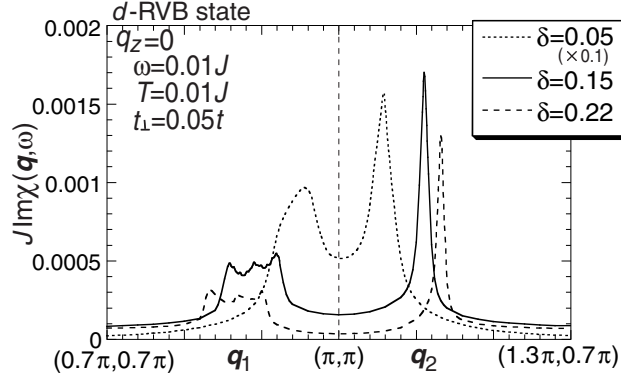


Fig. 3.  $q$ -dependence of  $\text{Im}\chi(\mathbf{q}, \omega)$  for several choices of  $\delta$  in the  $d$ -RVB state. The peak height at  $\mathbf{q}_2^{\text{DIC}}$  is larger than that at  $\mathbf{q}_1^{\text{DIC}}$  about 1.5, 3.5 and 4 times for  $\delta = 0.05, 0.15$  and  $0.22$ , respectively. The result for  $\delta = 0.05$  is multiplied by 0.1. The rough topped DIC-peak at  $\mathbf{q}_1^{\text{DIC}}$  for  $\delta = 0.15$  and  $0.22$  may be due to the artifact of the present calculation and should be interpreted as a smooth one.

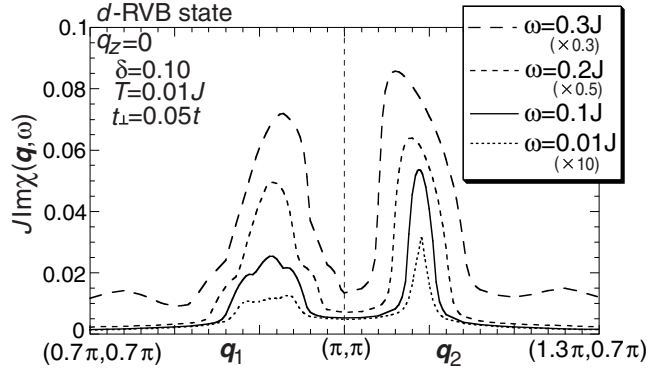


Fig. 4.  $q$ -dependence of  $\text{Im}\chi(q, \omega)$  for several choices of  $\omega$  in the  $d$ -RVB state. The results for  $\omega = 0.3J$ ,  $0.2J$  and  $0.01J$  are multiplied by 0.3, 0.5 and 10, respectively.

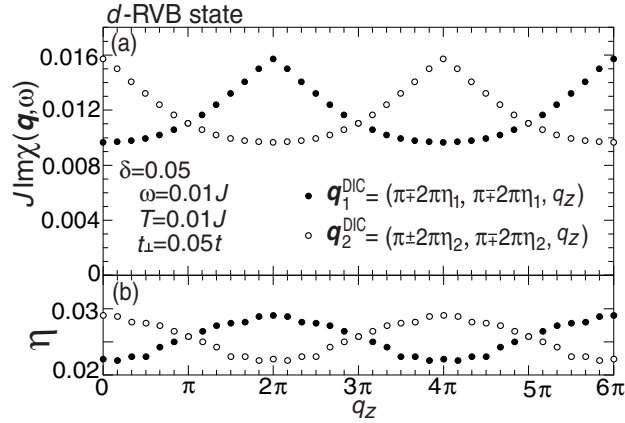


Fig. 5. (a)  $q_z$ -dependence of the peak height of the DIC-peaks at  $\mathbf{q}_1^{\text{DIC}} = (\pi \mp 2\pi\eta_1, \pi \mp 2\pi\eta_1, q_z)$  (solid circles) and  $\mathbf{q}_2^{\text{DIC}} = (\pi \pm 2\pi\eta_2, \pi \mp 2\pi\eta_2, q_z)$  (open circles) in the  $d$ -RVB state. (b)  $q_z$ -dependence of  $\eta_1$  (solid circles) and  $\eta_2$  (open circles).

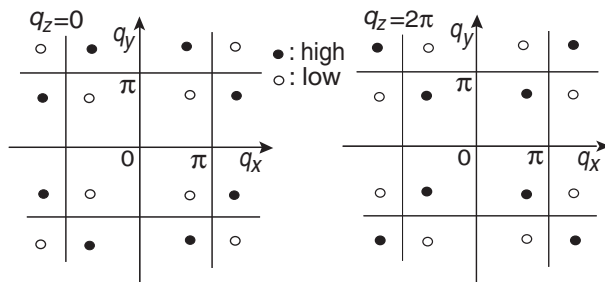


Fig. 6. Schematic figure on how the fourfold symmetry in the DIC-peaks is broken in the inplane momentum space for  $q_z = 0$  (left panel) and  $q_z = 2\pi$  (right panel). Solid circles (open circles) indicate the positions of the DIC-peaks with higher (lower) intensity.

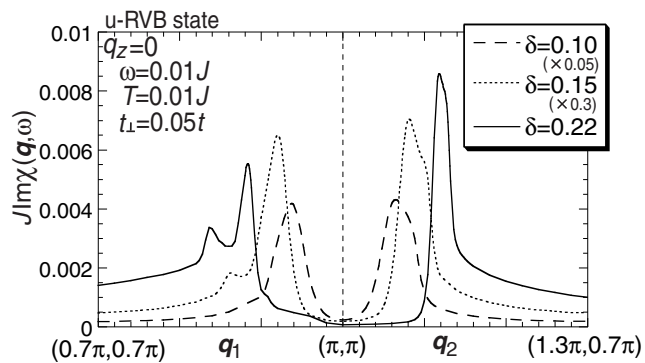


Fig. 7.  $q$ -dependence of the  $\text{Im}\chi(\mathbf{q}, \omega)$  for several choices of  $\delta$  in the u-RVB state (the state without the  $d$ -wave gap). The results for  $\delta = 0.10$  and  $0.15$  are multiplied by  $0.05$ ,  $0.3$ , respectively.

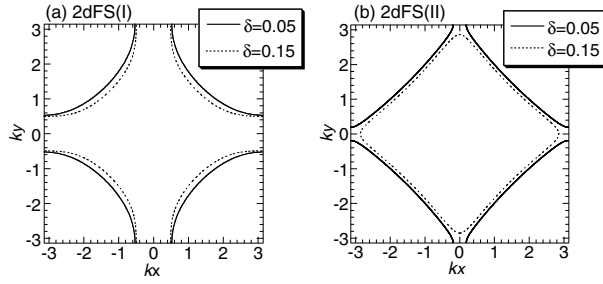


Fig. 8. (a) The 2dFS(I), which is realized in YBCO.<sup>24)</sup> (b) The 2dFS(II), which was used in the previous theoretical studies for LSCO.<sup>25–27)</sup>

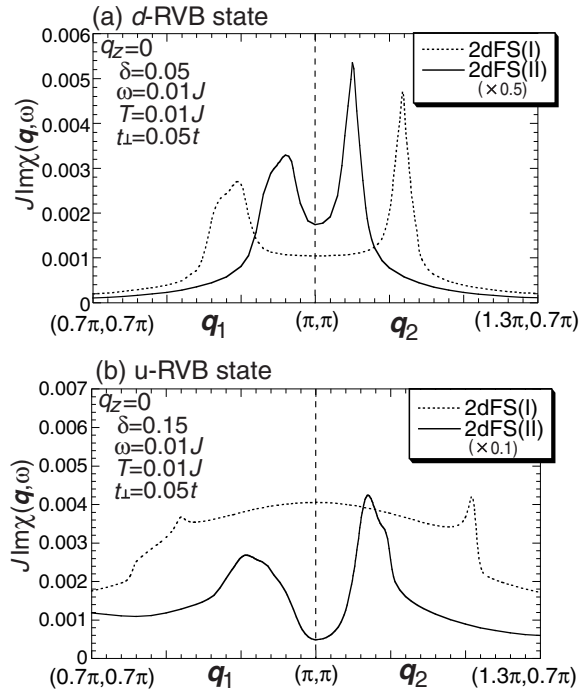


Fig. 9.  $q$ -dependence of  $\text{Im}\chi(\mathbf{q}, \omega)$  for other FSs, the 2dFS(I) and the 2dFS(II), in the  $d$ -RVB state (a) and in the  $u$ -RVB state (b). Note that the interlayer hopping integral  $t_{\perp}$  is included. The results for the 2dFS(II) in the  $d$ -RVB state and in the  $u$ -RVB state are multiplied by 0.5 and 0.1, respectively.